Earth and Planetary Science Letters 396 (2014) 66–77

Contents lists available at ScienceDirect

Earth and Planetary Science Letters

www.elsevier.com/locate/epsl

Continental weathering following a Cryogenian glaciation: Evidence from calcium and magnesium isotopes

Simone A. Kasemann [a,*], Philip A.E. Pogge von Strandmann [b], Anthony R. Prave [c], Anthony E. Fallick [d], Tim Elliott [e], Karl-Heinz Hoffmann [f]

[a] Department of Geosciences and MARUM-Center for Marine Environmental Sciences, University of Bremen, 28334 Bremen, Germany
[b] Institute of Earth and Planetary Sciences, UCL and Birkbeck, University of London, Gower Street, London WC1E 6BT, UK
[c] Earth Sciences, University of St. Andrews, St. Andrews KY16 9AL, UK
[d] Scottish Universities Environmental Research Centre, East Kilbride G75 OQF, UK
[e] Department of Earth Sciences, University of Bristol, Bristol BS8 1RJ, UK
[f] Geological Survey of Namibia, P.O. Box 2168, Windhoek, Namibia

ARTICLE INFO

Article history:
Received 10 September 2013
Received in revised form 20 March 2014
Accepted 21 March 2014
Available online 19 April 2014
Editor: G. Henderson

Keywords:
calcium isotopes
magnesium isotopes
continental weathering
cap carbonates
Neoproterozoic

ABSTRACT

A marked ocean acidification event and elevated atmospheric carbon dioxide concentrations following the extreme environmental conditions of the younger Cryogenian glaciation have been inferred from boron isotope measurements. Calcium and magnesium isotope analyses offer additional insights into the processes occurring during this time. Data from Neoproterozoic sections in Namibia indicate that following the end of glaciation the continental weathering flux transitioned from being of mixed carbonate and silicate character to a silicate-dominated one. Combined with the effects of primary dolomite formation in the cap dolostones, this caused the ocean to depart from a state of acidification and return to higher pH after climatic amelioration. Differences in the magnitude of stratigraphic isotopic changes across the continental margin of the southern Congo craton shelf point to local influences modifying and amplifying the global signal, which need to be considered in order to avoid overestimation of the worldwide chemical weathering flux.

1. Introduction

The response of the Earth system to recent changes in forcing parameters has attracted much attention. The response to and recovery from a hypothesised ultra-greenhouse state following the global glaciations of the Neoproterozoic represent one of the most acute tests of feedbacks within the Earth system to maintain an equable environment. Such events are marked geologically by deposition worldwide of 'cap carbonate' (Hoffman and Schrag, 2002), a distinctive rock layer that directly overlies glacial deposits or glaciated surfaces (Hoffman and Schrag, 2002; James et al., 2001; Kennedy, 1996; Kennedy et al. 1998, 2001a, 2001b; Williams, 1979).

Although cap carbonates are recognised as a fingerprint of the icehouse-to-greenhouse transition (Hoffman et al., 1998), no consensus exists as to their causal mechanism or the atmospheric–oceanic conditions under which they formed. A widely held view is that elevated atmospheric CO_2 would have generated extreme greenhouse conditions, acidified the post-glacial ocean, increased surface temperatures and precipitation and, as a consequence, continental weathering and riverine transport. This in turn led to enhanced rock (silicate) weathering thereby augmenting CO_2 consumption, increasing ocean alkalinity and pH, and, ultimately, lowering temperatures.

Stratigraphic trends in the stable isotope compositions of the cap carbonates are distinctive and largely consistent with the model described above. Carbon isotopes initially display a sharp negative excursion followed by recovery to more positive values. Even though lively debate remains regarding the exact cause of this excursion, many studies have shown the overall isotopic trends to be stratigraphically systematic and of global significance (e.g. Halverson et al., 2005). Further, concomitant negative boron isotope excursions in post-glacial carbonates have been used in a recent approach to address ocean pH fluctuations during the transition from icehouse to greenhouse states (Kasemann et al., 2010).

Having reconstructed ocean pH conditions for the older and younger Cryogenian pan-glacial states and identified a temporary

* Corresponding author. Tel.: +49 (0)421 218 65930.
E-mail addresses: skasemann@marum.de (S.A. Kasemann), p.strandmann@ucl.ac.uk (P.A.E. Pogge von Strandmann), ap13@st-andrews.ac.uk (A.R. Prave), t.fallick@suerc.gla.ac.uk (A.E. Fallick), Tim.Elliott@bristol.ac.uk (T. Elliott), khhoffmann@mme.gov.na (K.-H. Hoffmann).

http://dx.doi.org/10.1016/j.epsl.2014.03.048
0012-821X/

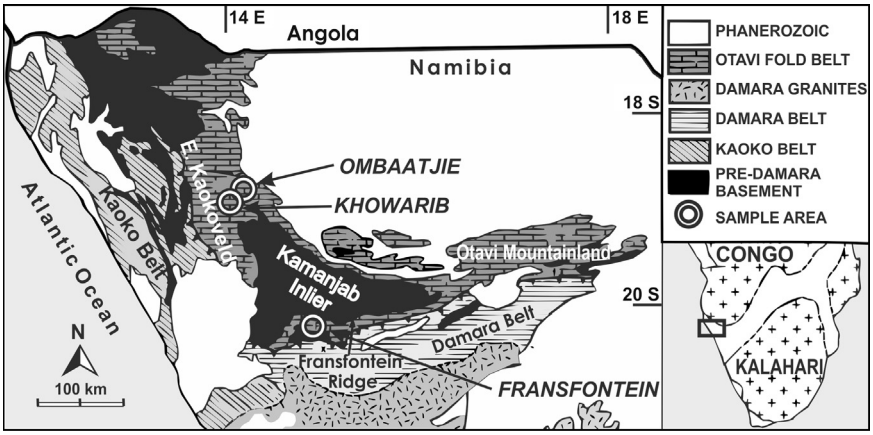

Fig. 1. Generalised geological map of northern Namibia showing location of three Neoproterozoic carbonate sections (modified after Kasemann et al., 2010). See text for discussion.

ocean acidification event for the younger interglacial (Kasemann et al., 2010), this study deals with the next critical step in deciphering Cryogenian environmental conditions: to resolve the discrepancy between having an acidic ocean whilst maintaining relatively high rates of carbonate sedimentation, and how the Earth system recovered from the extreme ocean pH conditions. The combined application of calcium and magnesium isotopes provides unique insight into the evolution of continental weathering, ocean alkalinity, and carbonate sedimentation under these unusual conditions.

1.1. Background

Chemical weathering of continental silicates consumes atmospheric CO_2, and acts as a climate-moderating process (e.g. Kump et al., 2000). In addition, weathering delivers carbonate and metal ions to the oceans (Berner et al., 1983, 1990; Kump et al., 2000; Walker et al., 1981) where they are removed via precipitation of calcium carbonate with implications for ocean alkalinity (Archer et al., 2000; Dessert et al., 2003; Gaillardet et al., 1999). Calcium and magnesium are key components in both chemical weathering reactions (e.g. Berner et al., 1983, 1990; Kump et al., 2000; Walker et al., 1981) and carbonate precipitation. In seawater and carbonates, their isotope ratios can change in response to large flux imbalances, fluctuations in ocean temperature, variations in mineralogy and rates of precipitation (e.g. Blättler et al., 2011; De la Rocha and DePaolo, 2000; Li et al., 2012; Pogge von Strandmann, 2008; Shen et al., 2009; Tang et al., 2008; Tipper et al., 2006a, 2006b; Zhu and Macdougall, 1998). Importantly, calcium and magnesium isotope ratios in ancient carbonates are strongly rock-buffered, hence largely unaffected by diagenesis (Fantle and DePaolo, 2007).

Ca and Mg have long modern oceanic residence times of ca. 1 Myr and 10 Myr, respectively (e.g. Berner and Berner, 1996; Holland, 1978). Accordingly, Ca and Mg isotopes preserved in Neoproterozoic interglacial carbonates can be used to trace and potentially quantify changes in continental weathering and ocean alkalinity and, consequently, yield insights into Earth's ancient climatic states. However, the isotope composition of seawater may still change over shorter time intervals if the influence of the driving factor is large enough and/or seawater exchange within the depositional basin is restricted (Holmden et al., 2012).

To test this, we have measured Ca and Mg isotope ratios on samples from carbonate units of the Neoproterozoic Otavi Group in NW Namibia (Fig. 1; Kasemann et al., 2005, 2010). These sections were deposited on the low-latitude continental margin of the southern Congo craton, represent different depositional facies (foreslope and platform) and contain a record of the younger Cryogenian (ca. 635 Ma) pan-glacial to greenhouse transition. The combined stable isotopic datasets for these sections enable us to construct and combine weathering/alkalinity, palaeo-pH and carbon chemistry profiles over a variety of water depths and settings for one depositional basin. Further, we can assess if Ca and Mg isotopes can be used: (i) as stratigraphic fingerprints recording characteristic trends specific to the younger Cryogenian (Marinoan) glaciation–deglaciation sequence; (ii) to identify their regional (local) and/or global significance; and (iii) to evaluate the nature and scale of chemical weathering and Earth system recovery during the Cryogenian climatic extremes.

2. Material and methods

2.1. Samples

Samples selected for this study were collected from the Neoproterozoic Otavi Group in NW Namibia (see Supplemental Online Material), and are the same samples on which Kasemann et al. (2005, 2010) previously obtained and reported C, O, and B isotope ratios (Supplementary Online Material). The sampled sections were from two well-exposed areas (Fig. 1), the eastern Kaokoveld carbonate platform (Ombaatjie and Khowarib sections) and the Fransfontein Ridge shelf-slope break (Fransfontein section), and define a transect from shallow- to deeper-marine settings across the palaeocontinental margin of the Congo craton (Kasemann et al., 2010). In addition, the sections capture the meltback phase of the younger Cryogenian (ca. 635 Ma) Ghaub Formation and the return to more moderate climatic conditions (Halverson et al., 2005; Hoffmann et al., 2004).

As noted in Kasemann et al. (2005, 2010), the sample localities have not experienced any degree of metamorphism and are only moderately deformed with broad and open folds. The rocks selected for isotope analyses preserve exquisite evidence of original depositional features and structures, are uniform and micritic in texture, and contain no observed evidence of secondary alteration or recrystallisation. Prior to isotope analyses, the quality of the samples was checked by scanning electron microscope (SEM) and trace element analyses using secondary ionisation mass spectrometry (SIMS), as detailed in Kasemann et al. (2005, 2010).

2.2. Analytical techniques

Calcium isotope ratios were determined in the laboratories of the Bristol Isotope Group (BIG) using the preparation technique, measurement routine and data collection method detailed in Kasemann et al. (2005, 2008) and Supplemental Online Material. Analyses were performed on a Thermo Finnigan Triton thermal

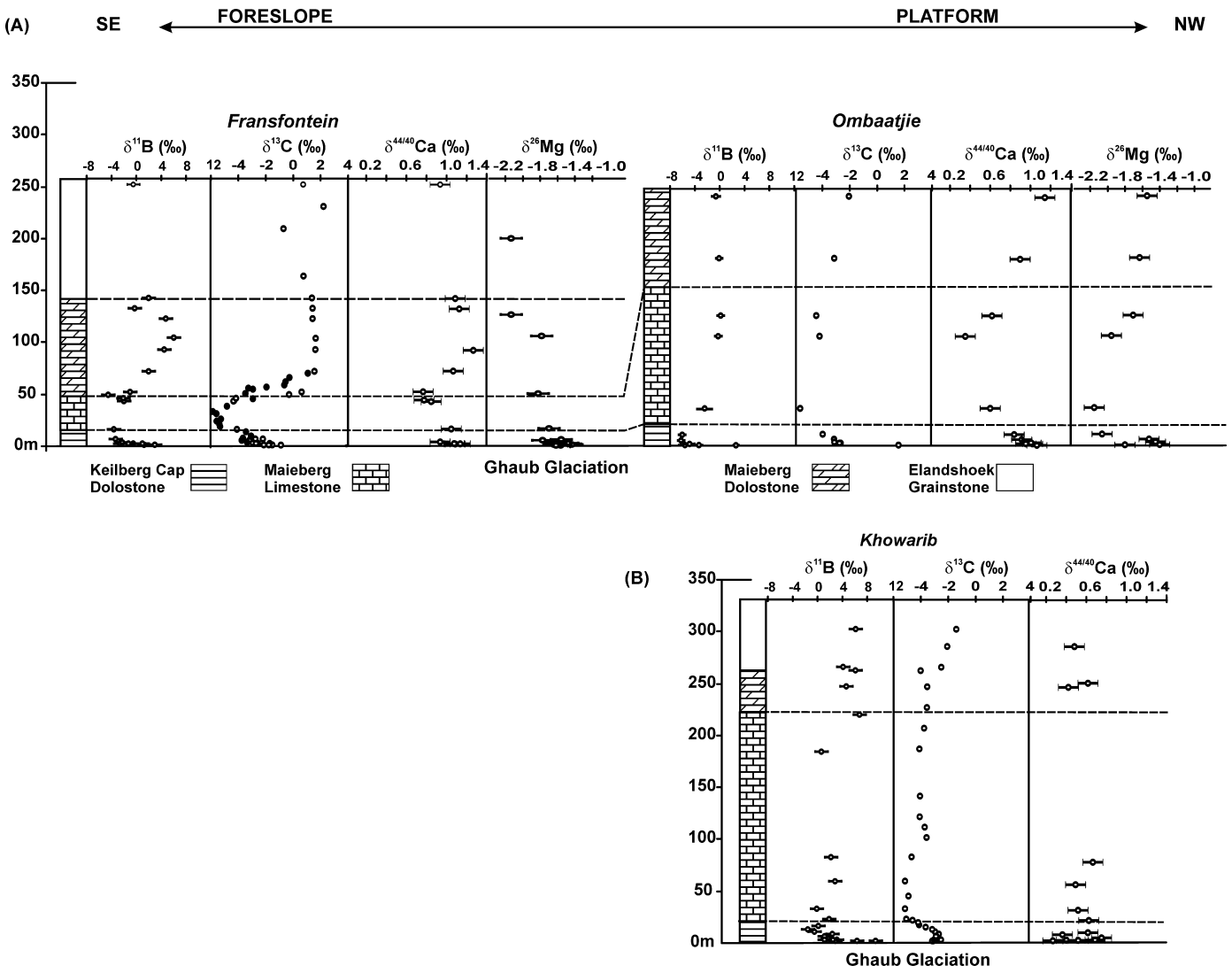

Fig. 2. Composite B, C, Mg and Ca isotope records for younger Cryogenian postglacial carbonate sections in Namibia. Transect from deeper- to shallow-marine settings, including (a) the Fransfontein section from the ridge shelf-slope break and the Ombaatjie section from the shallow shelf, as well as (b) the nearby shallow shelf Khowarib section.

ionisation mass spectrometer. Ca isotope ratios are given relative to NIST SRM 915a in the conventional $\delta^{44/40}$Ca (‰) notation. The $n(^{44}\text{Ca})/n(^{40}\text{Ca})$ ratio of the reference material for each analytical session was reproduced to within 0.1‰ (2σ), with an internal uncertainty of about 0.05‰ ($2\sigma_{\text{mean}}$). The uncertainty (2σ) on the isotope ratio of the samples is about 0.15‰.

Magnesium isotope ratios $n(^{26}\text{Mg})/n(^{24}\text{Mg})$ were measured using a Thermo Finnigan Neptune multicollector ICP-MS at Bristol University using an Elemental Scientific Inc. Apex-Q introduction system. Samples were analysed in a sample-standard bracketing technique, relative to the standard DSM-3 (Galy et al., 2003). Analyses and purification chemistry were performed as detailed in Pogge von Strandmann (2008) and Pogge von Strandmann et al. (2011). The external uncertainty (2σ) of the analyses is ±0.05‰ on δ^{26}Mg, as determined by repeated analyses of the same seawater sample ($n = 14$; chemistry = 14) (Foster et al., 2010) (see Supplemental Online Material for further details).

3. Results

The isotopic data are summarised in Fig. 2 (and Supplementary Online material; for detailed discussion of the C, O and B isotopic data see Kasemann et al., 2005, 2010). $\delta^{44/40}$Ca values for Fransfontein (foreslope; Figs. 2, 3) display a sinusoidal profile starting at 1.1‰ in the Keilberg cap-dolostone, decline to 0.8‰ in Maieberg dolostone, climb to 1.3‰ in limestone and end at 0.9‰ in the Elandshoek dolostones. The Ombaatjie (mostly inner-mid platform to peritidal settings) $\delta^{44/40}$Ca profile is bow-shaped and starts with a value of 1.1‰ in the cap dolostone, declines to 0.4‰ in the overlying deeper-marine rhythmites of the Maieberg limestone and returns steadily to 1.1‰ through the shallowing-upward trend of the inner-mid platform to peritidal Maieberg dolostones (Kasemann et al., 2005). In stark contrast, the $\delta^{44/40}$Ca values for the nearby Khowarib section (similar palaeoenvironmental setting as the Ombaatjie section) show relatively constant but rather low values (average of 0.51 ± 0.14‰, 1σ) with non-systematic scatter from 0.2 to 0.7‰ through the entire profile of 15 samples (Figs. 2, 3).

δ^{26}Mg profiles were constructed for the Keilberg–Maieberg cap-carbonate sequence at Fransfontein and Ombaatjie. In the former, δ^{26}Mg starts in the cap at −1.6‰, rises to −1.4‰ and declines through the Maieberg Formation to ca. −2.1‰ (Figs. 2, 3). In the latter, δ^{26}Mg starts at −1.8‰, increases to −1.4‰, then declines to −2.1‰ in Maieberg limestones before rising gradually to −1.5‰ through the rest of the formation.

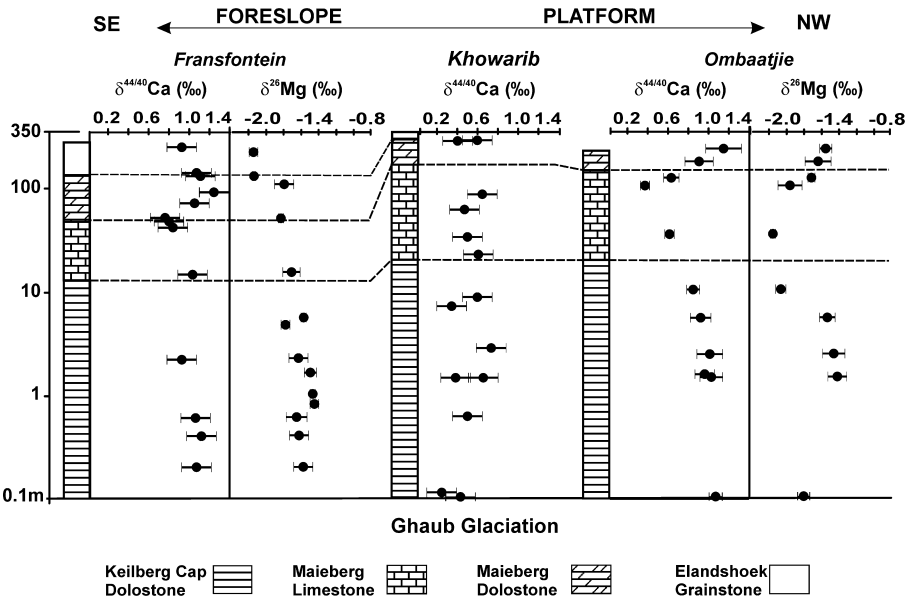

Fig. 3. Expanded (log-) view of the Mg and Ca isotope records for the younger Cryogenian postglacial carbonate sections in Namibia.

The Ca and Mg isotope inflections and trends do not correspond to or coincide with facies changes or lithostratigraphically defined formational boundaries. Consequently, the Ca and Mg isotope variation is not lithology-dependent nor does it reflect diagenetic alteration. Thus, we interpret the isotopic data as recording original seawater signals. This is not unexpected in that Ca and Mg are major elements in carbonate rocks but not usually in post-depositional fluids, and so their isotopic compositions are buffered against diagenetic change (Fantle and DePaolo, 2007; Silva-Tamayo et al., 2010b).

4. Discussions

4.1. Calcium isotope signals: local, regional or global?

Changes in the calcium isotope composition of seawater depend primarily on the net imbalance between calcium delivery to the ocean and burial in sediments as the flux of calcium increases/decreases in response to continental weathering and erosion (De la Rocha and DePaolo, 2000; Fantle and DePaolo, 2005; Zhu and Macdougall, 1998). Kasemann et al. (2005) documented a negative Ca isotope excursion of about 0.8‰ in the mostly shallow platform carbonate rocks (Ombaatjie section) in Namibia and interpreted that as reflecting a temporary imbalance between Ca input from continental weathering and Ca precipitation following the younger Cryogenian glacial. Subsequently, Silva-Tamayo et al. (2010a) obtained Ca isotope profiles for broadly equivalent successions in central-W Brazil and NW Canada (Fig. 4). They compared the isotopic pattern preserved in inner and outer platform carbonates from Brazil and Canada to the isotopic shallow platform pattern (Ombaatjie section) from Namibia and concluded that the Ca isotope perturbations were global and stratigraphically unique, and thus could be employed as a chemostratigraphic correlation tool. Examination of our Namibian data indicates otherwise: we find non-trivial differences in the Ca isotope variation across the palaeocontinental margin represented by the early Ediacaran Keilber–Maieberg Formation of the Otavi Group (Fig. 4).

Focussing solely on the well-constrained Keilberg–Maeiberg cap-carbonate sequences those at Fransfontein (which record a foreslope setting) and Ombaatjie (shallow platform setting) display what could be viewed uncritically as comparable, bow-shaped $\delta^{44/40}$Ca profiles (Fig. 4). However, even though both begin at ca. 1.1‰, smoothly decline, and then rise back to values of ca. 1‰, the nadir is significantly lower at Ombaatjie (ca. 0.4‰) than at Fransfontein (ca. 0.8‰). This reveals a statistically significant ($\alpha = 0.05$) difference in relative isotopic variation (at least 0.4‰) between the two localities. Further, the Ca isotope profile at Khowarib (a shallow marine platform section similar to Ombaatjie) shows data scattering non-systematically around 0.5‰. Thus, there is substantial and statistically significant variability in $\delta^{44/40}$Ca data along a single shallow platform-to-slope transect (mean $\delta^{44/40}$Ca ± measure of dispersion 1σ; Fransfontein: 1.01 ± 0.15‰, Ombaatjie: 0.86 ± 0.24‰, Khowarib: 0.51 ± 0.14‰), which refutes the claim by Silva-Tamayo et al. (2010a) that $\delta^{44/40}$Ca profiles are globally reproducible.

The observed differences in the $\delta^{44/40}$Ca profiles for the Namibian transect suggest a regional influence amplifying the global pattern. Especially, the considerably different and non-systematic pattern for the shallow platform Khowarib section reveals the potential of a strong local control on the $\delta^{44/40}$Ca profile. Because the Fransfontein section would have been located along the edge of an ocean-facing continental margin, and given the consistency of that section's $\delta^{44/40}$Ca data, we consider this profile to be the most reliable record of global ocean conditions. This, then, indicates that the extreme Ca isotope values (as low as 0.1‰ to as high as 2‰; Fig. 4) observed in the shallow marine sections from Brazil, Canada (Silva-Tamayo et al., 2010a) and Namibia (Kasemann et al., 2005), are signals recording local modifications, and show that the temporary global shift of ~0.5‰ in the Fransfontein section (from 0.8‰ to 1.3‰) can be magnified to as much as 2‰ (Fig. 4). Consequently, our results counsel prudence before applying Ca isotope stratigraphy as a tool to correlate Neoproterozoic postglacial carbonate successions, and question the reliability of $\delta^{44/40}$Ca profiles to differentiate between the interglacial successions. In addition, while investigating global Ca mass balance evolution and weathering flux predictions, care has to be taken in choosing a $\delta^{44/40}$Ca pattern that is minimally influenced by local factors.

4.2. Calcium and magnesium isotope signals: environmental implications

The local control on the $\delta^{44/40}$Ca pattern does, however, provide a unique opportunity to improve our understanding of, and ability to reconstruct, the environmental conditions associated

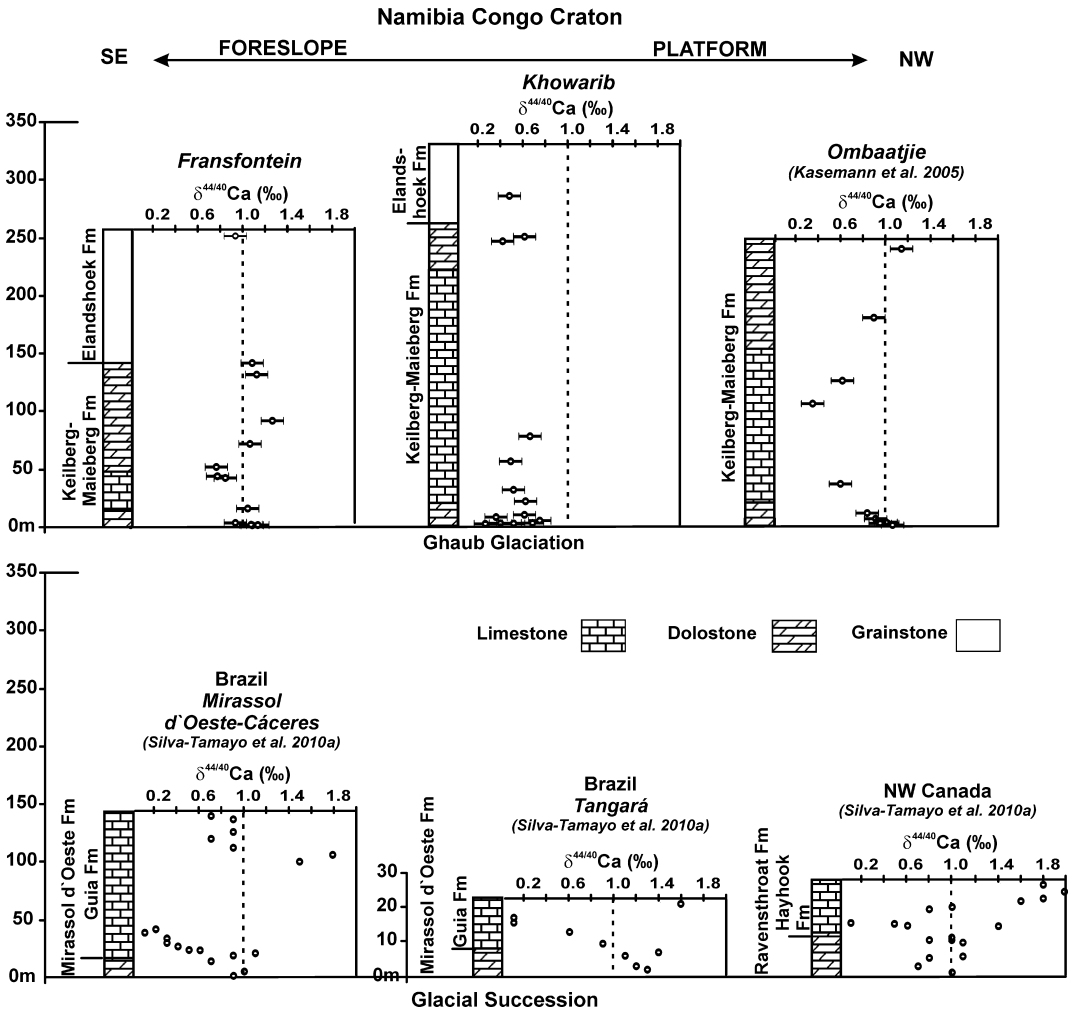

Fig. 4. Ca isotope records of the Keilberg–Maieberg formations in NW Namibia and the coeval postglacial carbonate successions in Brazil and NW Canada from Silva-Tamayo et al. (2010a).

with extreme Neoproterozoic climatic changes. Factors that could have influenced the Ca isotope composition of the Neoproterozoic oceans, apart from changes in the continental weathering flux (and regime), include the rate of carbonate precipitation as well as mineralogy (e.g. calcite/aragonite), and ocean temperature and pH (Fig. 5). Hence, considering the scenarios proposed for the formation of cap carbonates, the Ca isotope composition of carbonate precipitates would certainly change:

(i) Alkalinity and temperature changes

It has been proposed that cap carbonates owe their origin to upwelling of deep basinal alkaline water during deglaciation (Grotzinger and Knoll, 1995; Ridgwell et al., 2003). Another view is that Cryogenian surface ocean temperature increased from −1.5 °C to 30 °C (Higgins and Schrag, 2003; Pierrehumbert, 2004) during deglaciation. In the former scenario, stimulation of carbonate precipitation would involve an increased Ca output and, hence, a positive Ca isotope excursion. In the latter, since Ca isotope fractionation decreases with increasing temperature (Gussone et al., 2005; Marriott et al., 2004; Nägler et al., 2000), the temperature effect should also drive a positive Ca isotope shift of ∼0.6‰ (Gussone et al., 2005) during cap carbonate precipitation, because carbonate is ubiquitously isotopically lighter than the Ca ion in aqueous solution. In contrast, our $\delta^{44/40}$Ca data show a declining, rather than increasing, trend.

(ii) Precipitation rate changes

Alternatively, experimental studies on spontaneous calcite precipitation have demonstrated that Ca isotope fractionation values

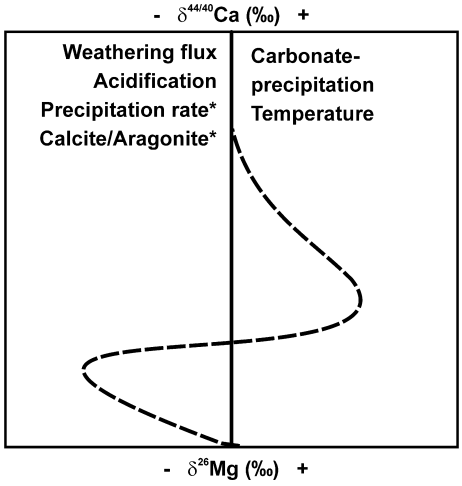

Fig. 5. Schematic overview on the relative shift in Ca and Mg isotope composition in carbonates as a function of factors that could have been present in the Neoproterozoic world. *Changes in the isotope composition induced by the precipitation rate and mineralogy (aragonite/calcite) are only valid for calcium. Changes in the Mg isotope ratio induced by temperature have been so far only observed for carbonates precipitated under laboratory conditions (see text for discussion).

between calcite and aqueous Ca ($\Delta^{44/40}Ca_{calcite\text{-}aqueous}$) are positively correlated (i.e. increase) with the precipitation rate, although the effect becomes weaker with increasing temperature (Tang et

al., 2008). This positive rate-dependence on the Ca isotope fractionation is, especially at high precipitation rates, counterbalanced by the negative temperature-dependence and thus would not be able to produce the smooth and temporary declining isotope trend. Instead, it could only explain the non-systematic scatter and low $\delta^{44/40}$Ca of the shallow-marine Khowarib section marked by a thick Keilberg–Maieberg carbonate sequence (Figs. 2, 3).

(iii) Changes induced by mineralogy

Since aragonite has a Ca isotope ratio 0.6‰ lower than cogenetic calcite (Gussone et al., 2005), a global shift in carbonate mineralogy from calcite to aragonite is capable of producing the negative Ca isotope excursion observed in the Cryogenian successions. Such a scenario would require dominantly calcite mineralogy at the start of the deglaciation followed by principal aragonite precipitation up-section in the Keilberg–Maieberg, where the return to more positive values would document the initiation of a new global ocean steady state with a higher seawater Ca isotope composition (or, if it is temporary, a shift back to dominant calcite mineralogy). However, the sedimentary record and the lithology-independent Ca isotope variations do not support this. So far, a systematic study on Ca isotope fractionation in dolomite has not been published and insufficient Ca isotope data on dolomites have been reported (Holmden, 2009; Kasemann et al., 2005; Steuber and Buhl, 2006) to assess if a shift from potentially primary dolomite at the start of cap deposition to calcite and/or aragonite is capable of producing the Ca isotope excursion. Then again, such a shift is not supported by the lithology-independent Ca isotope variation.

(iv) Changes induced by variation in pH and continental weathering

A temporary acidification scenario during which carbonate deposition decreases due to ocean acidification and subsequently increases due to weathering feedbacks (Payne et al., 2010) would result in an initial decrease in the carbonate depositional flux, accompanied by Ca accumulation in the seawater and a decrease in the Ca isotope composition, followed by an increase in carbonate deposition and return to a steady state and higher Ca isotope values. Boron isotope data obtained from the same samples offer support to such a scenario: Kasemann et al. (2010) modelled a marked ocean acidification event compatible with elevated postglacial pCO_2 concentration for the younger deglaciation period. However, due to the limited amount of seafloor carbonate, carbonate dissolution together with a disruption of carbonate precipitation would by itself not be capable of producing the observed negative isotope excursion (Blättler et al., 2011). During the Phanerozoic, a change in composition of weathered lithology could change the Ca isotope composition of seawater when, for example, Ca isotope fractionation in marine shelled organisms drives carbonate rocks to more negative values compared to the average igneous rock ($\delta^{44/40}$Ca ~ 0.9‰, see DePaolo, 2004 and references therein). However, Neoproterozoic carbonate rocks do not contain marine shelled organisms and the $\delta^{44/40}$Ca values (e.g. $\delta^{44/40}$Ca ~ 1‰, Ombaatjie and Fransfontein Fms, supplementary data) are on average higher than modern oozes ($\delta^{44/40}$Ca ~ 0.4‰) and similar to average igneous rocks (e.g. $\delta^{44/40}$Ca 1 to 1.4‰, Tipper et al., 2006a).

Similar to Ca, the Mg isotope composition of seawater (Fig. 5) is predominantly controlled by a change in riverine Mg isotope flux (Tipper et al., 2006b), along with the ratio between the two seawater sinks: hydrothermal removal (which scavenges Mg quantitatively, and hence causes no isotope fractionation), and carbonate formation, which preferentially takes up light ^{24}Mg, and therefore drives seawater isotopically heavier ($\Delta^{26/24}Mg_{calcite\text{-}aqueous}$ ~ −2.7‰, $\Delta^{26/24}Mg_{dolomite\text{-}aqueous}$ ~ −1.8 to −2.7‰ depending of the type of dolomite mineralisation; Galy et al., 2002; Higgins and Schrag, 2010; Tipper et al., 2006b). In addition, a temporary ocean acidification event could decrease the Mg isotope ratio while a parallel rise in temperature would again drive an increase in δ^{26}Mg during cap carbonate precipitation (observed for carbonates precipitated under laboratory conditions; Li et al., 2012). On the other hand, δ^{26}Mg values in seawater are more dependent on the dominant type of weathering rock, i.e. silicates versus carbonates, and preliminary studies in modern weathering environments indicate further significant isotope fractionation between mineral residue and solution (e.g. Pogge von Strandmann et al., 2008) potentially generated via silicate soil formation (Pogge von Strandmann et al., 2012; Tipper et al., 2006b, 2010) and biological productivity in soils or rivers (Black et al., 2006; Bolou-Bi et al., 2010). Silicate rocks from the continental crust display δ^{26}Mg values ranging from −0.5 to +0.9‰ (Li et al., 2010; Liu et al., 2010; Shen et al., 2009; Tipper et al., 2006b), while Cryogenian carbonate rocks tend to be lower (δ^{26}Mg between −2.2 and −1.1‰) with an average Mg isotopic composition ~−1.6‰, similar to reported Phanerozoic (δ^{26}Mg: −4.4 to −1‰, Tipper et al., 2006b) and Ediacaran carbonate data (δ^{26}Mg: −2.3 to −0.8‰, Pokrovsky et al., 2011).

Focussing on a temporary imbalance between weathering influx and precipitation as the main driver for both isotope excursions, continental weathering in the greenhouse aftermath of a glaciation would not only drive enhanced weathering of silicates but also of carbonates. While carbonate weathering does not sequester CO_2 on geological timescales, its alkalinity flux might account for the deposition of the postglacial cap carbonates (Higgins and Schrag, 2003; Hoffman and Schrag, 2002). It has been recognised that alkalinity release from silicate weathering was neither rapid enough nor sufficient to account for cap carbonates; also, that the dissolution of carbonate minerals would be enhanced during deglaciation (lower temperature and emerged platforms) (Le Hir et al., 2009; Higgins and Schrag, 2003; Hoffman and Schrag, 2002) while maximum silicate weathering is reached after cap carbonate deposition (following melting and transgression) (Kasemann et al., 2005; Nogueira et al., 2007).

The assumed change from carbonate-dominated to silicate-dominated weathering is apparent in the relationship and timing of the Ca and Mg isotope pattern for the Ombaatjie platform section. Both $\delta^{44/40}$Ca and δ^{26}Mg display a bow-shaped negative shift indicating the temporary elevated weathering flux. However, the Mg excursion starts and terminates first with the nadir at the transition between the Keilberg cap dolostones and Maieberg limestones, whereas the nadir in the Ca excursion occurs stratigraphically higher (Fig. 2) and above where aragonite fan pseudomorphs are locally preserved. Consequently, the termination of cap dolostone sedimentation does not mark the end of enhanced weathering (Kennedy et al., 2001b), but may reflect the change from carbonate-dominated (low δ^{26}Mg) to silicate-dominated (low $\delta^{44/40}$Ca) weathering as carbonate platforms are drowned by rising sea level (Hoffman and Schrag, 2002).

That continental weathering is indeed the principal driver for the Ca and Mg isotope variation is also implied by the distinctive relationship between C, Ca, and Mg isotopes, in particular in the Ombaatjie section (Fig. 6). It is remarkable that for the Keilberg–Maieberg Formation, with the consistent exception of the contact sample (OBTJ 43) between the glacial and the Keilberg sequence (see also discussion of Fig. 2 in Kasemann et al., 2005), there are robust relationships between the carbon isotopic composition of the carbonates and the corresponding Ca and Mg isotope ratios (Fig. 6). The trends are plausibly linear: for $\delta^{44/40}$Ca versus $\delta^{13}C_{carb}$, $r = 0.79$, >99% significant for $n = 10$ (Fig. 6(a)); for δ^{26}Mg versus $\delta^{13}C_{carb}$, $r = 0.82$, >99% significant for $n = 9$ (Fig. 6(b)). This strongly suggests that Ca, Mg and C isotopes are coupled through continental (silicate + carbon-bearing rocks) weathering. As mentioned above, silicate weathering draws down CO_2 but carbonate weathering does not remove CO_2 from the atmosphere in the long term, permitting at least partial decoupling of some of the

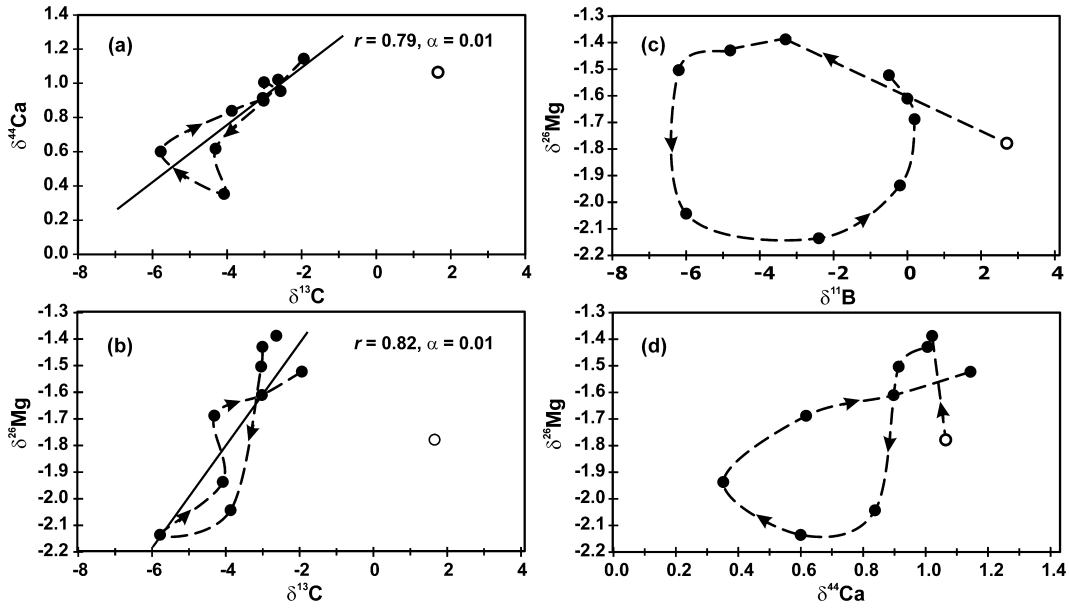

Fig. 6. Crossplots of B, C, Mg and Ca isotope data for the postglacial carbonate rocks from the Ombaatjie platform section. The arrows in (a) to (d) indicate the stratigraphic sequence of samples from the base to the top of the postglacial section. The open circle represents the basal Keilberg cap contact sample. The correlation coefficient r in (a) and (b) is given for the postglacial rocks excluding the contact sample.

C isotope excursion from the recovery to more normal atmospheric CO_2 levels. In the interpretation of Fig. 6 it is crucial to remember that the negative $\delta^{13}C_{carb}$ excursions during the Neoproterozoic are considered global and representative of "primary perturbation of the surface carbon cycle" with a "characteristic timescale of 10^5 to 10^6 years" (Johnston et al., 2012). Explanations invoking isotope resetting during diagenesis, or a massive pool of dissolved (or, indeed, particulate) organic carbon, have been convincingly ruled out by these authors. Thus, moving from $\delta^{13}C_{carb}$ close to zero to values of $-6‰$ or less likely implies an Earth system shifting between two end-member modes of operation. The first is similar to that of today with a balance between delivery of carbon to the ocean and sequestration of carbon in sediments at a ratio of carbonate C to organic C of 4 to 1. The second is where there is an enhanced input to the ocean of isotopically light carbon, presumed by Johnston et al. (2012) to be either methane or ancient organic matter in sediments delivered by weathering.

The first end-member mode would be characterised by carbonate $\delta^{44/40}Ca > 1.2‰$ (and perhaps as high as $\sim 1.4‰$), and $\delta^{26}Mg > -1.4‰$ (and perhaps $\sim -1.0‰$). The second mode, by contrast, has $\delta^{44/40}Ca \leqslant 0.4‰$ and $\delta^{26}Mg \leqslant -2.1‰$ (Fig. 6(d)). We note that these latter values are not inconsistent with an enhanced riverine contribution from weathering of organic-rich sedimentary lithologies. Within this general scenario, the relationships illustrated in Fig. 6 then reflect various stages of the Earth system intermediate between the two end members, with the proviso that absolute values of $\delta^{44/40}Ca$ and $\delta^{26}Mg$ are subject to modification by the processes already discussed above. The straight lines in Fig. 6 then represent, in a certain sense, the locus of mixing ratios (or transitions between end member modes of operation): note that we do not claim to have described (or measured) actual end members, only transitions towards them. The linearity is explained by relatively constant proportions of C : Ca : Mg in the ocean input, and the deviations of individual points from strict linearity may reflect various processes, including short-term differences in the input terms (e.g. decoupling of input sources), modification of isotope ratios by other processes as described above, and buffering of isotope ratio changes for the various elements depending on the different oceanic residence times. Such 'noise' may be elucidated by consideration of $\delta^{44/40}Ca$ versus $\delta^{26}Mg$. High $\delta^{26}Mg$ is always accompanied by high $\delta^{44/40}Ca$ at times of low continental weathering, and low $\delta^{26}Mg$ is always accompanied by low $\delta^{44/40}Ca$ at times of enhanced continental weathering. However, high $\delta^{44/40}Ca$ is not always accompanied by high $\delta^{26}Mg$, and intermediate $\delta^{26}Mg$ can have high or low $\delta^{44/40}Ca$ perhaps signifying the changing influence of carbonate weathering (Fig. 6(d)).

4.3. Modelling seawater calcium and magnesium isotope excursions

To test the extent to which the postulated changes in the continental weathering input and regime (i.e. episodes dominated by carbonate and silicate) are capable of producing the observed Ca and Mg isotope excursions, and also to elucidate timing and magnitude, we use a series of dynamic box models. The oceanic box models were calculated assuming that the sources of Ca to the oceans are continental weathering and hydrothermal fluids, and the sole source of Mg is continental weathering (in accordance with mass balance models for the Phanerozoic, e.g. Blättler et al., 2011; Payne et al., 2010; Pogge von Strandmann et al., 2013). The common sink of Ca and Mg is net carbonate burial, while Mg is additionally removed via hydrothermal activity (which scavenges Mg quantitatively, and hence causes no isotope fractionation), and dolomite formation (high Mg sink compared to calcite). Both the calcium and magnesium cycles are modelled by taking the isotope ratios and magnitudes of the fluxes and isotope fractionation factors between sinks and sources from modern mass balance estimates (see Blättler et al., 2011; Tipper et al., 2006b and references therein) (Fig. 7). For the calcium mass balance equation the hydrothermal flux was set to 2.0×10^{12} mol yr^{-1} with $\delta^{44/40}Ca = 0.9‰$, the basic river flux to 2.3×10^{13} mol yr^{-1} with an initial $\delta^{44/40}Ca$ of $1.0‰$ to adjust for initial steady state conditions, and the initial oceanic calcium reservoir was set to 1.4×10^{19} mol; $\Delta^{44/40}Ca_{carbonate\text{-}aqueous} = -0.8‰$. The mass balance equation for the magnesium model takes account of 5.6×10^{12} mol yr^{-1} basic river flux with an initial $\delta^{26}Mg$ of $-1.0‰$ and an initial oceanic magnesium reservoir of 7.3×10^{19} mol. Magnesium removal by carbonate precipitation is taken to be constant at $-2.7‰$ (equal to $\Delta^{26/24}Mg_{calcite\text{-}aqueous}$), and hence independent of the mineralogy of carbonate output (i.e. we do not assume different fractionation factors for dolomite or limestone precipitation;

Parameter	Ca: value and unit	Mg: value and unit
Initial		
River flux	2.3×10^{13} mol yr^{-1}	5.6×10^{12} mol yr^{-1}
River isotope composition	1.0‰	−1.0‰
Perturbed		
Isotope composition silicate flux endmember	1.2‰	−0.3‰
Isotope composition carbonate flux endmember	0.8‰	−2.5‰
$\text{Seawater}_{\text{initial}}$	1.4×10^{19} mol	7.3×10^{19} mol
Hydrothermal flux	2.0×10^{12} mol yr^{-1}	
Hydrothermal isotope composition	0.9‰	
Carbonate precipitation $\Delta_{\text{carb-aqueous}}$	−0.8‰	−2.7‰

Fig. 7. Parameter values used in the oceanic box model. Model parameters are derived from Blättler et al. (2011), DePaolo (2004), Higgins and Schrag (2010), Holland (2005), Milliman (1993), Tipper et al. (2006a, 2006b), Wilkinson and Algeo (1989). Initial river isotope ratios as well as the Ca seawater reservoir were taken from modern with subsequent small adjustments to achieve data-valid starting compositions. Seawater and output flux values respond to model adjustments and changes over time.

Higgins and Schrag, 2010). This accounts for the observed broad range in δ^{26}Mg caused by the type of dolomite mineralisation and the facies-independent isotope pattern. The sink for both isotope systems is calculated as a partition coefficient, i.e. it is responsive to the seawater concentration. In the model, both elemental cycles are linked through the common riverine flux sources, carbonate and silicate rocks. The oceanic Mg and Ca isotope ratio then evolves as the balance of the carbonate and silicate mixture of the younger interglacial surface runoff changes through time. Bearing in mind the different element abundances of the two main lithologies, the average end-member silicate flux is taken as having $\delta^{44/40}\text{Ca} \sim 1.2‰$ and $\delta^{26}\text{Mg} \sim -0.3‰$, whereas the average end-member carbonate flux has $\delta^{44/40}\text{Ca} \sim 0.8‰$ and $\delta^{26}\text{Mg} \sim -2.5‰$ (Tipper et al., 2006a, 2006b).

Initially, the steady-state balance of the system was perturbed by changing the continental source flux linked to the assumed change from carbonate- to silicate-dominated weathering. The Ca isotope excursion observed on the slope (Fransfontein section), and considered to be the most reliable record of global ocean conditions, can be best matched by a combined (50% each) carbonate plus silicate weathering flux of 9× (all fluxes are given as a multiplier of the present day flux; see Holland, 2005) for about 500 kyr, followed by a dominant silicate weathering pulse of 6× for 1 Myr. In contrast, an initial, 500 kyr-lasting carbonate plus silicate weathering flux of 20×, followed by a dominant silicate weathering pulse of 15× for 1 Ma would be necessary to produce the Ca isotope excursion observed on the platform (Ombaatjie section) (Fig. 8(a), (b)). The inferred twofold increase in weathering fluxes emphasises the magnified global shift in the local platform signal as a result of a restricted (embayed) basin or water body size rather than actually higher fluxes. Furthermore, to produce the initial δ^{26}Mg increase right at the base of the cap and to fully decouple the Ca and Mg isotope excursion we would have to assume high primary dolomite formation for the first e.g. 100 kyr (cap dolostone, 85% Mg sink: Keilberg is primary dolomite, i.e. was a large Mg sink at the time of deposition) followed by primary carbonate (calcite and/or aragonite) precipitation (present day 15–28% Mg sink; Holland, 2005; Tipper et al., 2006b). Alternatively, an exclusive silicate weathering influx of e.g. 20× for 1 Myr would also produce the general isotope pattern observed on the platform, but in contrast to what we observe in the isotope record, the nadir in $\delta^{44/40}$Ca would occur earlier than the one in δ^{26}Mg (Fig. 8(c)). A much lower silicate weathering influx of e.g. 5× for 1 Myr, would still be capable of reproducing the Ca isotope pattern on the slope but would not be sufficient to generate a significant Mg pattern (Fig. 8(d)). Note, that we have ignored the potential effects of changing temperature and mineralogy in order to investigate the effects of weathering alone.

In an attempt to infer CO_2 consumption during increased silicate weathering in the post-panglacial environment, we use the calculated river fluxes from the oceanic box model. Our simplistic calculation is based on the assumption that, as in modern rivers, silicate weathering rate and CO_2 consumption rate stay linear (Gaillardet et al., 1999). A CO_2 consumption of 6.9×10^{19} mol in 1.5 Myr is inferred by applying the modern ratio of silicate weathering flux (Ca and Mg) and CO_2 consumption fluxes on the modelled silicate weathering flux from Fransfontein (silicate weathering increases post-snowball to 4.5x, then 6x). This is a ∼5-fold increase in silicate weathering compared to the "normal" modern rate of 8.7×10^{12} mol C yr^{-1} lasting for about 1.5 Myr (only continental weathering; Gaillardet et al., 1999).

Beside the discussion on rock (silicate) weathering augmenting CO_2 consumption and controlling ocean pH in the younger Cryogenian glacial aftermath, the timescale and rate of 'cap carbonate' precipitation is a matter of on-going debate (e.g. Hoffman et al., 2007). In our model we found that a time period of at least 3 Myr is needed to drive the entire Ca–Mg isotope perturbation on both the slope and platform Keilberg–Maieberg carbonate sections, assuming modern ocean residence times for Ca and Mg. This time period is in excellent agreement with a model calculation on Ca isotope oscillation in Brazilian cap carbonates (Silva-Tamayo et al., 2010a) and U–Pb ages from China (Condon et al., 2005). Focussing on the postglacial Keilberg cap dolostones, our model predicts a deposition period of ∼100 kyr and a sedimentation rate between 0.15 to 0.2 mm yr^{-1} for Keilberg cap dolostone going from slope to platform. In addition, a uniform deposition period of ∼1 Myr with an average sedimentation rate ranging from 0.03 mm yr^{-1} on the slope to 0.14 and potentially up to 0.22 mm yr^{-1} on the platform are implied for the Maieberg limestone. However, timescale and rate of deposition of Keilberg cap dolostone inferred from the model are in sharp contrast with rapid deposition of <10 kyr (between 2000 and 10 000 years; Higgins and Schrag, 2003; Hoffman et al., 2007; Kennedy et al., 2001b) and an average sedimentation rate of 0.01 m yr^{-1} (3.8 to 19.0 mm yr^{-1}) as inferred by climate models (Hoffman et al., 2007) and sedimentological features implying fast deposition (e.g. Hoffman, 2011). While our timescale of cap dolostone deposition exceeds the duration inferred by climate models, it, however, correlates with magnetostratigraphic data suggesting that cap dolostones accumulated over several hundreds of thousands of years (Kilner et al., 2005; Trindade et al., 2003) implying either much slower glacial meltdown, or cap dolostone accumulation surpassing the period of glacio-eustatic rise (Hoffman et al., 2007). Note that our oceanic box model is not designed to highly resolve the time of cap dolostone deposition but to reproduce the overall Ca–Mg isotope pattern. To critically assess the geochemical evolution of the Cryogenian–Ediacaran ocean–atmosphere system and to account for palaeogeography and palaeobathymetry, as well as for other environmental conditions and feedback mechanisms, more sophisticated Earth system models are needed. In addition, to explicitly simulate and assess the changing influx and significance of continental silicate weathering (especially for the Keilberg cap

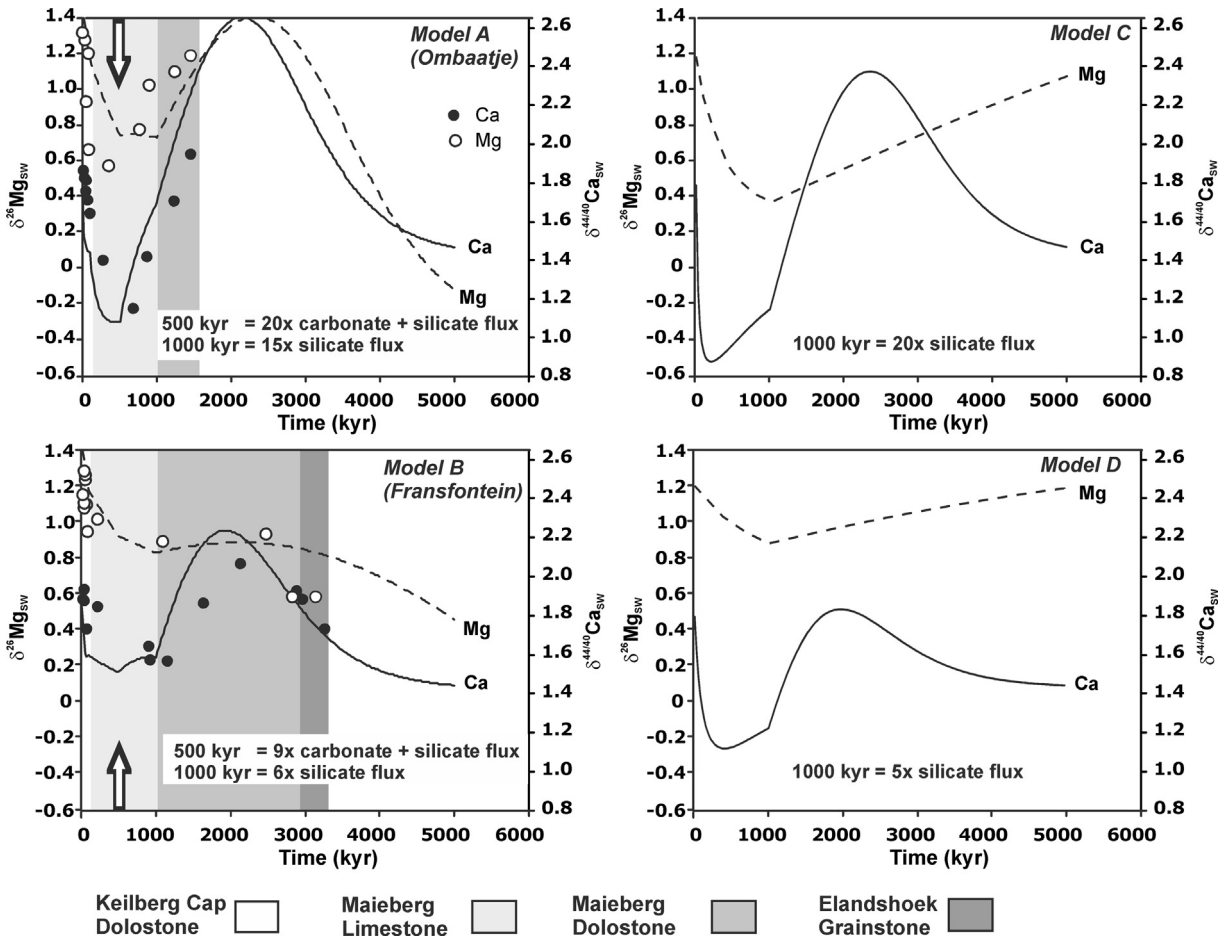

Fig. 8. A combined plot of the dynamic box model outcome for the Mg and Ca isotope excursion through time and the actual Mg and Ca isotope excursion (converted seawater values) observed on the shelf-slope break (Fransfontein) and platform (Ombaatjie). The model outcome for A and B is given for the weathering scenario proposed to best match the Mg and Ca isotope excursion from slope to platform: a combined carbonate plus silicate weathering flux respectively of 9 and 20 times present day for about 500 kyr, followed by a dominant silicate weathering pulse of respectively 6 and 15 times present day for 1 Myr, as well as high primary dolomite formation for the first e.g. 100 kyr (cap dolostone, 85% Mg sink) followed by primary calcite formation. The arrows indicate the timing of the expected change in weathering regime. The relative position of the analysed Mg and Ca isotope data and Formation boundaries on the time axis is given by the stratigraphic sequence; assumed timescale and rate of deposition can only be regarded as mean values. Models C and D represent the outcome for an exclusive silicate weathering influx of 20× for 1 Myr and 5× for 1 Myr, respectively (see text for discussion).

dolostone deposition), additional proxy data, e.g. lithium isotopes, are needed which respond solely to silicate weathering over short timescales.

4.4. Continental weathering and ocean pH

If, as suggested by our data, the younger Cryogenian pan- to interglacial transition was indeed a time of enhanced continental weathering, then the concomitant flux of alkalinity into the seawater must have enabled the ocean to return from an acidification event to a state of pH normalcy. The linkage between enhanced continental weathering and buffered ocean pH is emphasised by the observation that the transient ocean acidification event, indicated by the negative δ^{11}B excursion of the Keilberg–Maieberg sequence (Kasemann et al., 2010), is essentially tracked by δ^{13}C, $\delta^{44/40}$Ca and δ^{26}Mg (Fig. 2) and, by implication, continental weathering. As reported in Kasemann et al. (2010), the δ^{11}B-ocean pH profiles from the palaeocontinental margin are comparable in cyclicity. However, similar to the regional differences in the magnitude of the Ca and Mg isotope excursion, slight regional differences in timing of the B isotope excursion exist. In case of the shelf-slope break section (Fransfontein) – our most reliable record of global ocean conditions – the δ^{11}B-ocean pH excursion is essentially tracked by δ^{13}C and $\delta^{44/40}$Ca. The recovery from the ocean acidification event starts within the Maieberg limestones and hence, in time with the change in the weathering regime and maximum silicate weathering flux, indicating the connection between ocean pH, continental weathering and potentially pCO_2 (Fig. 9). On the shallow-marine platform section (Ombaatjie), the nadir in δ^{11}B-ocean pH occurs already in the Keilberg cap dolostones and well before the nadir in δ^{13}C, $\delta^{44/40}$Ca and δ^{26}Mg (Fig. 2). In fact, there is a progressive change between δ^{11}B versus δ^{13}C (see Fig. 2 in Kasemann et al., 2005), $\delta^{44/40}$Ca and especially δ^{26}Mg (Fig. 6(c)). The smooth "clockwise" trend highlights different periods when either B changed and Mg did not, or Mg changed and B remained constant. This difference in timing was initially interpreted as a potential disconnection between ocean pH and atmospheric CO_2 (Kasemann et al., 2005) and hence weathering. Instead, the early nadir in δ^{11}B and the partial decoupling from δ^{13}C, $\delta^{44/40}$Ca and δ^{26}Mg at the platform could be the result of a combination of processes linked to the general change in the weathering regime and the local scale of the weathering signal. Considering the magnified continental weathering signal on the platform, the early nadir in δ^{11}B-ocean pH implies that the pH of the seawater was locally influenced by the enhanced rise in alkalinity, which must have buffered the shallow and potentially restricted water body on the platform first and foremost, as compared to the open ocean on the shelf-slope break. Additionally,

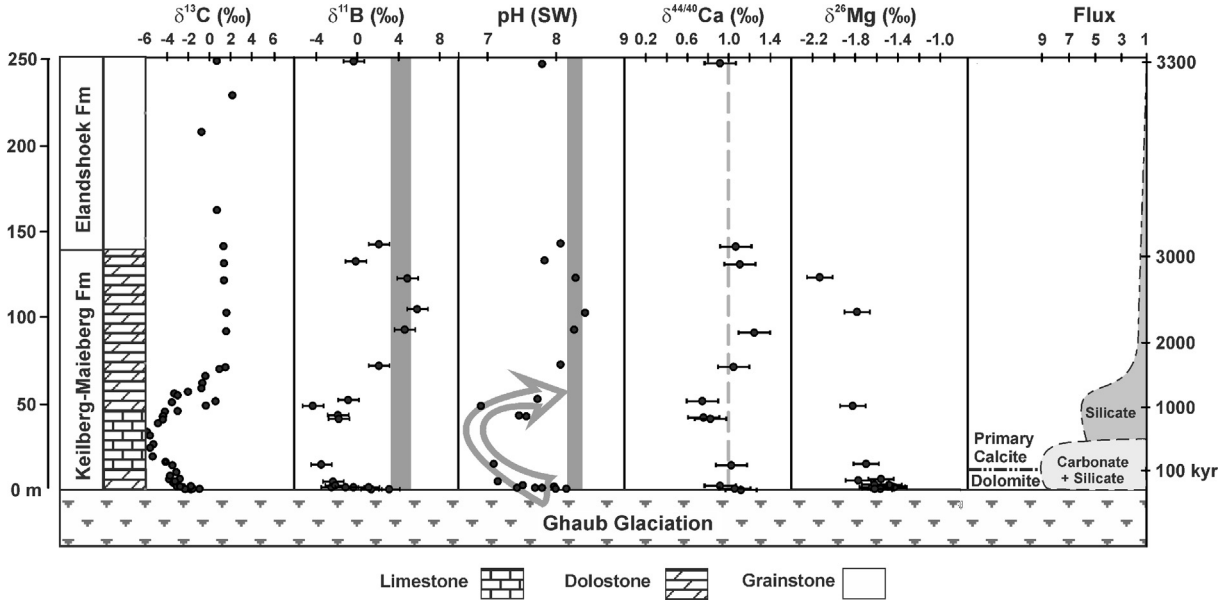

Fig. 9. Composite boron, carbon, calcium and magnesium (B, C, Ca, Mg) isotope record together with palaeo-pH and continental weathering flux reconstructions for the post-Ghaub carbonate succession at Fransfontein (foreslope) in northern Namibia (modified after Kasemann et al., 2010). Grey area marks average B isotope composition and ocean pH conditions of inferred Neoproterozoic climatic normalcy. Arrow indicates inferred transient ocean acidification event. For a detailed discussion on the boron and pH data see Kasemann et al. (2010).

while the dominant carbonate weathering flux at the outset is able to increase alkalinity and buffer pH, it would not remove CO_2 from the atmosphere in the long term.

5. Conclusions

Calcium and magnesium isotope patterns, preserved in the Otavi Group carbonate rocks from Namibia, indicate an enhanced continental weathering influx following the demise of the younger Cryogenian (ca. 635 Ma) glaciation. This observation is in general accordance with results gained from broadly equivalent successions in Brazil and Canada by Silva-Tamayo et al. (2010a), signifying a global Ca perturbation of the ocean via flux imbalances in response to continental weathering. Yet, our study identifies significant differences in the magnitude of the Ca isotope excursions between the different basins and notably even along the single palaeocontinental margin transect of the Congo craton in Namibia. A simple oceanic box model based on the Ca and Mg isotope data from Namibia revealed a twofold increase in the calculated weathering flux for the platform setting compared to the slope setting. Instead of implying variable weathering fluxes across the palaeocontinental margin, the more pronounced platform signal (Ombaatjie section) rather suggests a local influence of a restricted basin or water body, potentially amplifying the global pattern represented by the slope (Fransfontein) section. The non-systematic scatter in the second platform section (Khowarib) points to an additional strong local control on the Ca isotope signal due to potential differences in rates of carbonate precipitation, carbonate supersaturation and/or temperature. Consequently, Ca isotope profiles are not globally reproducible and not a reliable chemostratigraphic correlation tool, and extreme regional isotope signals can lead to an overestimate of the global chemical weathering flux. Observed differences in the timing of the Ca and Mg isotope excursion in both of our platform and slope sections are best explained by primary dolomite formation during Keilberg cap dolostone sedimentation together with a change from carbonate- to silicate-dominated continental weathering as carbonate platforms are drowned by rising sea level. Our box model implies an initial carbonate plus silicate weathering flux and a change in the continental weathering regime above the cap dolostone sedimentation and during deposition of the deeper-water limestone rhythmites of the lower Maieberg Formation. Dominant silicate weathering is reached stratigraphically higher in the Maieberg limestones near and/or above where aragonite fans occur and in the highstand sequence (Hoffman, 2011) of the Maieberg dolostones. The enhanced continental weathering flux and concomitant flux of alkalinity into the seawater must have enabled the Earth system to recover from low ocean pH conditions and to maintain carbonate sedimentation even under acidic ocean conditions. Consequently, the documentation of combined proxy records of $\delta^{44/40}$Ca and δ^{26}Mg with δ^{11}B and δ^{13}C allows to better delineate the response and recovery from a hypothesised postglacial, ultra-greenhouse state and how this impacts on the Earth system's capacity to maintain an equable environment.

Acknowledgements

This work was funded by a Natural Environment Research Council New Investigator Award (NE/C507529/1) to SAK. PPvS is funded by NERC Research Fellowship NE/1020571/1. We are grateful to C. Taylor for the sample preparation in the analytical facilities at Bristol University. The manuscript has benefited from careful reviews by A. Rooney and two anonymous reviewers, and editorial handling from G. Henderson.

Appendix A. Supplementary material

Supplementary material related to this article can be found online at http://dx.doi.org/10.1016/j.epsl.2014.03.048.

References

Archer, D.E., Winguth, A., Lea, D., Mahowald, N., 2000. What caused the glacial/interglacial atmospheric pCO_2 cycles? Rev. Geophys. 38, 159–189.

Berner, R.A., 1990. Global CO_2 degassing and the carbon-cycle – comment on Cretaceous Ocean Crust at DSDP Site-417 and Site-418 – carbon uptake from weathering vs loss by magmatic outgassing. Geochim. Cosmochim. Acta 54, 2889–2890.

Berner, E.K., Berner, R.A., 1996. Global Environment: Water, Air and Geochemical Cycles. Prentice Hall, Upper Saddle River, N.J.

Berner, R.A., Lasaga, A.C., Garrels, R.M., 1983. The carbonate–silicate geochemical cycle and its effect on atmospheric carbon–dioxide over the past 100 million years. Am. J. Sci. 283, 641–683.
Black, J.R., Yin, Q.Z., Casey, W.H., 2006. An experimental study of magnesium-isotope fractionation in chlorophyll – a photosynthesis. Geochim. Cosmochim. Acta 70, 4072–4079.
Blättler, C.L., Jenkyns, H.C., Reynard, L.M., Henderson, G.M., 2011. Significant increases in global weathering during Oceanic Anoxic Events 1a and 2 indicated by calcium isotopes. Earth Planet. Sci. Lett. 309, 77–88.
Bolou-Bi, E.B., Poszwa, A., Leyval, C., Vigier, N., 2010. Experimental determination of magnesium isotope fractionation during higher plant growth. Geochim. Cosmochim. Acta 74, 2523–2537.
Condon, D., Zhu, M., Bowring, S., Wang, W., Yang, A., Jin, Y., 2005. U–Pb ages from the Neoproterozoic Doushantuo Formation, China. Science 308, 95–98.
De La Rocha, C.L., DePaolo, D.J., 2000. Isotopic evidence for variations in the marine calcium cycle over the Cenozoic. Science 289, 1176–1178.
DePaolo, D.J., 2004. Calcium isotopic variations produced by biological, kinetic, radiogenic and nucleosynthetic processes. Rev. Mineral. Geochem. 55, 255–288.
Dessert, C., Dupre, B., Gaillardet, J., Francois, L.M., Allegre, C.J., 2003. Basalt weathering laws and the impact of basalt weathering on the global carbon cycle. Chem. Geol. 202, 257–273.
Fantle, M.S., DePaolo, D.J., 2005. Variations in the marine Ca cycle over the past 20 million years. Earth Planet. Sci. Lett. 237, 102–117.
Fantle, M.S., DePaolo, D.J., 2007. Ca isotopes in carbonate sediment and pore fluid from ODP site 807A: the Ca^{2+}(aq)–calcite equilibrium fractionation factor and calcite recrystallization rates in Pleistocene sediments. Geochim. Cosmochim. Acta 71, 2524–2546.
Foster, G.L., Pogge von Strandmann, P.A.E., Rae, J.W.B., 2010. Boron and magnesium isotopic composition of seawater. Geochem. Geophys. Geosyst. 11, Q08015. http://dx.doi.org/10.1029/2010GC003201.
Gaillardet, J., Dupré, B., Louvat, P., Allegre, C.J., 1999. Global silicate weathering and CO_2 consumption rates deduced from the chemistry of large rivers. Chem. Geol. 159, 3–30.
Galy, A., Bar-Matthews, M., Halicz, L., O'Nions, R.K., 2002. Mg isotopic composition of carbonate: insight from speleothem formation. Earth Planet. Sci. Lett. 201, 105–115.
Galy, A., Yoffe, O., Janney, P.E., Williams, R.W., Cloquet, C., Alard, O., Halicz, L., Wadwha, M., Hutcheon, I.D., Ramon, E., Carignan, J., 2003. Magnesium isotope heterogeneity of the isotope standard SRM 980 and new reference materials for magnesium-isotope-ratio measurements. J. Anal. At. Spectrom. 18, 1352–1356.
Grotzinger, J.P., Knoll, A.H., 1995. Anomalous carbonate precipitates: is the Precambrian the key to the Permian? Palaios 10, 578–596.
Gussone, N., Böhm, F., Eisenhauer, A., Dietzel, M., Heuser, A., Teichert, B.M.A., Reitner, J., Wörheide, G., Dullo, W.-C., 2005. Calcium isotope fractionation in calcite and aragonite. Geochim. Cosmochim. Acta 69, 4485–4494.
Halverson, G.P., Hoffman, P.F., Schrag, D.P., Maloof, A.C., Rice, A.H.N., 2005. Toward a Neoproterozoic composite carbon-isotope record. Geol. Soc. Am. Bull. 117, 1181–1207.
Higgins, J.A., Schrag, D.P., 2003. Aftermath of a snowball Earth. Geochem. Geophys. Geosyst. 4, 1028. http://dx.doi.org/10.1029/2002GC000403.
Higgins, J.A., Schrag, D.P., 2010. Constraining magnesium cycling in marine sediments using magnesium isotopes. Geochim. Cosmochim. Acta 74, 5039–5053.
Hoffman, P.F., 2011. Strange bedfellows: glacial diamictite and cap carbonate from the Marinoan (635 Ma) glaciation in Namibia. Sedimentology 58, 57–119.
Hoffmann, K.H., Condon, D.J., Bowring, S.A., Crowley, J.L., 2004. U–Pb zircon date from the Neoproterozoic Ghaub formation, Namibia: constraints on Marinoan glaciations. Geology 32, 817–820.
Hoffman, P.F., Halverson, G.P., Domack, E.W., Husson, J.M., Higgins, J.A., Schrag, D.P., 2007. Are basal Ediacaran (635 Ma) post-glacial "cap-dolostones" diachronous? Earth Planet. Sci. Lett. 258, 114–131.
Hoffman, P.F., Kaufman, A.J., Halverson, G.P., Schrag, D.P.A., 1998. Neoproterozoic snowball Earth. Science 281, 1342–1346.
Hoffman, P.F., Schrag, D.P., 2002. The snowball Earth hypothesis: testing the limits of global change. Terra Nova 14, 129–155.
Holland, H.D., 1978. The Chemistry of the Atmosphere and the Oceans. Wiley–Interscience, New York.
Holland, H.D., 2005. Sea level, sediments and the composition of seawater. Am. J. Sci. 305, 220–239.
Holmden, C., 2009. Ca isotope study of Ordovician dolomite, limestone, and anhydrite in the Williston Basin: implications for subsurface dolomitization and local Ca cycling. Chem. Geol. 268, 180–188.
Holmden, C., Papanastassiou, D.A., Blanchon, P., Evans, S., 2012. $\delta^{44/40}$Ca variability in shallow water carbonates and the impact of submarine groundwater discharge on Ca-cycling in marine environments. Geochim. Cosmochim. Acta 83, 179–194.
James, N.P., Narbonne, G.M., Kyser, T.K., 2001. Late Neoproterozoic cap carbonates: Mackenzie mountains, Northwestern Canada: precipitation and global glacial meltdown. Can. J. Earth Sci. 38, 1229–1262.
Johnston, D.T., Macdonald, F.A., Gill, B.C., Hoffman, P.F., Schrag, D.P., 2012. Uncovering the Neoproterozoic carbon cycle. Nature 483, 320–323.
Kasemann, S.A., Hawkesworth, C.J., Prave, A.R., Fallick, A.E., Pearson, P.N., 2005. Boron and calcium isotope composition in Neoproterozoic carbonate rocks from Namibia: evidence for extreme environmental change. Earth Planet. Sci. Lett. 231, 73–86.
Kasemann, S.A., Prave, A.R., Fallick, A.E., Hawkesworth, C.J., Hoffmann, K.-H., 2010. Neoproterozoic ice ages, boron isotopes and ocean acidification: implications for a snowball Earth. Geology 38, 775–777.
Kasemann, S.A., Schmidt, D.N., Pearson, P.N., Hawkesworth, C.J., 2008. Biological and ecological insights into Ca isotopes in planktic foraminifers as a palaeotemperature proxy. Earth Planet. Sci. Lett. 271, 292–302.
Kennedy, M.J., 1996. Stratigraphy, sedimentology, and isotopic geochemistry of Australian Neoproterozoic postglacial cap dolostones: deglaciation, δ^{13}C excursions, and carbonate precipitation. J. Sediment. Res. 66, 1050–1064.
Kennedy, M.J., Christie-Blick, N., Prave, A.R., 2001a. Carbon isotopic composition of Neoproterozoic glacial carbonates as a test of paleoceanographic models for snowball Earth phenomena. Geology 29, 1135–1138.
Kennedy, M.J., Christie-Blick, N., Sohl, L.E., 2001b. Are Proterozoic cap carbonates and isotopic excursions a record of gas hydrate destabilization following Earth's coldest intervals? Geology 29, 443–446.
Kennedy, M.J., Runnegar, B., Prave, A.R., Hoffmann, K.-H., Arthur, M.A., 1998. Two or four Neoproterozoic glaciations? Geology 26, 1059–1063.
Kilner, B., MacNiocaill, C., Brasier, M., 2005. Low-latitude glaciation in the Neoproterozoic of Oman. Geology 33, 413–416.
Kump, L.R., Brantley, S.L., Arthur, M.A., 2000. Chemical weathering, atmospheric CO_2 and climate. Annu. Rev. Earth Planet. Sci. 28, 611–667.
Le Hir, G., Donnadieu, Y., Goddéris, Y., Pierrehumbert, R.T., Halverson, G.P., Macouin, M., Nédélec, A., Ramstein, G., 2009. The snowball Earth aftermath: exploring the limits of continental weathering processes. Earth Planet. Sci. Lett. 277, 453–463.
Li, W., Chakraborty, S., Beard, B.L., Romanek, C.S., Johnson, C.M., 2012. Magnesium isotope fractionation during precipitation of inorganic calcite under laboratory conditions. Earth Planet. Sci. Lett. 333, 304–316.
Li, W.-Y., Teng, F.-Z., Ke, S., Rudnick, R.L., Gao, S., Wu, F.-Y., Chappell, B.W., 2010. Heterogeneous magnesium isotopic composition of the upper continental crust. Geochim. Cosmochim. Acta 74, 6867–6884.
Liu, S.-A., Teng, F.-Z., He, Y., Ke, S., Li, S., 2010. Investigation of magnesium isotope fractionation during granite differentiation: implication for Mg isotopic composition of the continental crust. Earth Planet. Sci. Lett. 297, 646–654.
Marriott, C.S., Henderson, G.M., Belshaw, N.S., Tudhope, A.W., 2004. Temperature dependence of delta Li-7, delta Ca-44 and Li/Ca during growth of calcium carbonate. Earth Planet. Sci. Lett. 222, 615–624.
Milliman, J.D., 1993. Production and accumulation of calcium carbonate in the ocean: budget of a nonsteady state. Glob. Biogeochem. Cycles 7, 927–957.
Nägler, T.F., Eisenhauer, A., Müller, A., Hemleben, C., Kramers, J., 2000. The δ^{44}Ca temperature calibration on fossil and cultured *Globigerinoides sacculifer*: new tool for reconstruction of past sea surface temperatures. Geochem. Geophys. Geosyst. 1, 1052. http://dx.doi.org/10.1029/2000GC000091.
Nogueira, A.C.R., Riccomini, C., Sial, A.N., Moura, C.A.V., Trindade, R., Fairchild, T.R., 2007. Carbon and strontium isotope fluctuations and paleoceanographic changes in the late Neoproterozoic Araras carbonate platform, southern Amazon craton, Brazil. Chem. Geol. 237, 168–190.
Payne, J.L., Turchyn, A.V., Paytan, A., DePaolo, D.J., Lehrmann, D.J., Yu, M., Wei, J., 2010. Calcium isotope constraints on the end-Permian mass extinction. Proc. Natl. Acad. Sci. 107, 8543–8548.
Pierrehumbert, R.T., 2004. High levels of carbon dioxide necessary for the termination of global glaciations. Nature 429, 646–649.
Pogge von Strandmann, P.A.E., 2008. Precise magnesium isotope measurements in core-top planktic and benthic Foraminifera. Geochem. Geophys. Geosyst. 9. http://dx.doi.org/10.1029/2008GC002209.
Pogge von Strandmann, P.A.E., Burton, K.W., James, R.H., van Calsteren, P., Gislason, S.R., Sigfusson, B., 2008. The influence of weathering processes on riverine magnesium isotopes in a basaltic terrain. Earth Planet. Sci. Lett. 276, 187–197.
Pogge von Strandmann, P.A.E., Elliott, T., Marschall, H.R., Coath, C.D., Lai, Y.J., Jeffcoate, A.B., Ionov, D.A., 2011. Variations of Li and Mg isotope ratios in bulk chondrites and mantle xenoliths. Geochim. Cosmochim. Acta 75, 5247–5268.
Pogge von Strandmann, P.A.E., Jenkyns, H.C., Woodfine, R.G., 2013. Lithium isotope evidence for enhanced weathering during Oceanic Anoxic Event 2. Nat. Geosci. 6, 668–672.
Pogge von Strandmann, P.A.E., Opfergelt, S., Lai, Y.J., Sigfusson, B., Gislason, S.R., Burton, K.W., 2012. Lithium, magnesium and silicon isotope behaviour accompanying weathering in a basaltic soil and pore water profile in Iceland. Earth Planet. Sci. Lett. 339–340, 11–23.
Pokrovsky, B.G., Mavromatis, V., Pokrovsky, O.S., 2011. Co-variation of Mg and C isotopes in late Precambrian carbonates of the Siberian platform: a new tool for tracing the change in weathering regime? Chem. Geol. 290, 67–74.
Ridgwell, A.J., Kennedy, M.J., Caldeira, K., 2003. Carbonate deposition, climate stability, and Neoproterozoic ice ages. Science 302, 859–862.
Shen, B., Jacobsen, B., Lee, C.-T.A., Yin, Q.-Z., Morton, D.M., 2009. The Mg isotopic systematics of granitoids in continental arcs and implications for the role of chemical weathering in crust formation. Proc. Natl. Acad. Sci. 106, 20652–20657.
Silva-Tamayo, J.C., Nägler, T.F., Sial, A.N., Nogueira, A., Kyser, K., Riccomini, C., James, N.P., Narbonne, G.M., Villa, I.M., 2010a. Global perturbation of the marine Ca

isotopic composition in the aftermath of the Marinoan global glaciation. Precambrian Res. 182, 373–381.

Silva-Tamayo, J.C., Nägler, T.F., Villa, I.M., Kyser, K., Vieira, L.C., Sial, A.N., Narbonne, G.M., James, N.P., 2010b. Global Ca isotope variations in ca. 0.7 Ga old postglacial successions. Terra Nova 22 (3), 188–194. http://dx.doi.org/10.1111/j.1365-3121.2010.00933.x.

Steuber, T., Buhl, D., 2006. Calcium-isotope fractionation in selected modern and ancient marine carbonates. Geochim. Cosmochim. Acta 70, 5507–5521.

Tang, J., Dietzel, M., Böhm, F., Köhler, S.J., Eisenhauer, A., 2008. Sr^{2+}/Ca^{2+} and $^{44}Ca/^{40}Ca$ fractionation during inorganic calcite formation: II. Ca isotopes. Geochim. Cosmochim. Acta 72, 3733–3745.

Tipper, E.T., Gaillardet, J., Louvat, P., Capmas, F., White, A.F., 2010. Mg isotope constraints on soil pore-fluid chemistry: evidence from Santa Cruz, California. Geochim. Cosmochim. Acta 74, 3883–3896.

Tipper, E.T., Galy, A., Bickle, M.J., 2006a. Riverine evidence for a fractionated reservoir of Ca and Mg on the continents: implications for the oceanic Ca cycle. Earth Planet. Sci. Lett. 247, 267–279.

Tipper, E.T., Galy, A., Gaillardet, J., Bickle, M.J., Elderfield, H., Carder, E.A., 2006b. The magnesium isotope budget of the modern ocean: constraints from riverine magnesium isotope ratios. Earth Planet. Sci. Lett. 250, 241–253.

Trindade, R.I.F., Font, E., D'Agrella-Filho, M.S., Nogueira, A.C.R., Riccomini, C., 2003. Low latitude and multiple geomagnetic reversals in the Neoproterozoic Puga cap carbonate, Amazon craton. Terra Nova 15, 441–446.

Walker, J.C.G., Hays, P.B., Kasting, J.F., 1981. A negative feedback mechanism for the long-term stabilization of the Earth's surface temperature. J. Geophys. Res. 86, 9776–9782.

Wilkinson, B.H., Algeo, T.J., 1989. Sedimentary carbonate record of calcium–magnesium cycling. Am. J. Sci. 289, 1158–1194.

Williams, G.E., 1979. Sedimentology, stable-isotope geochemistry and palaeoenvironment of dolostones capping late Precambrian glacial sequences in Australia. J. Geol. Soc. Aust. 26, 377–386.

Zhu, P., Macdougall, J.D., 1998. Calcium isotopes in the marine environment and the oceanic calcium cycle. Geochim. Cosmochim. Acta 62, 1691–1698.